Structures, origin and evolution of various carbon phases in the ureilite Northwest Africa 4742 compared with laboratory-shocked graphite

C. Le Guillou, J.N. Rouzaud, L. Remuzat, Albert Jambon, Michèle Bourot-Denise

Available online at www.sciencedirect.com
ScienceDirect
Geochimica et Cosmochimica Acta 74 (2010) 4167–4185
Geochimica et Cosmochimica Acta
www.elsevier.com/locate/gca

Structures, origin and evolution of various carbon phases in the ureilite Northwest Africa 4742 compared with laboratory-shocked graphite

C. Le Guillou [a,*], J.N. Rouzaud [a], L. Remusat [b], A. Jambon [c], M. Bourot-Denise [b]

[a] *Laboratoire de géologie de l'ENS, Paris, UMR8538 CNRS-ENS, 24 rue Lhomond, 75231 Paris Cedex 5, France*
[b] *Laboratoire de Minéralogie et Cosmochimie du Muséum, UMR CNRS 7202, Muséum National d'Histoire Naturelle, CP 52, 57 rue Cuvier, 75231 Paris Cedex 05, France*
[c] *Université Pierre et Marie Curie, Paris 6 & IPGP, UMR7154, 4 Place Jussieu, 75005 Paris, France*

Received 6 April 2009; accepted in revised form 12 March 2010; available online 22 April 2010

Abstract

Mineralogical structures of carbon phases within the ureilite North West Africa 4742, a recent find, are investigated at various scales by high-resolution transmission electron microscopy (HRTEM), Raman microspectrometry and X-ray diffraction. Ureilites are the most carbon-rich of all meteorites, containing up to 6 wt.% carbon. Diamond, graphite and so-called "amorphous carbon" are typically described, but their crystallographic relationships and respective thermal histories remain poorly constrained. We especially focus on the origin of "amorphous carbon" and graphite, as well as their relationship with diamond.

Two aliquots of carbon-bearing material were extracted: the insoluble organic matter (IOM) and the diamond fraction. We also compare the observed structures with those of laboratory-shocked graphite.

Polycrystalline diamond aggregates with mean coherent domains of about 40 nm are reported for the first time in a ureilite and TEM demonstrates that all carbon phases are crystallographically related at the nanometre scale.

Shock features show that diamond is produced from graphite through a martensitic transition. This observation demonstrates that graphite was present when the shock occurred and is consequently a precursor of diamond. The structure of what is commonly described as the "amorphous carbon" has been identified. It is not completely amorphous but only disordered and consists of nanometre-sized polyaromatic units surrounding the diamond. Comparison with laboratory-shocked graphite, partially transformed into diamond, indicates that the disordered carbon could be the product of diamond post-shock annealing.

As diamond is the carrier of noble gases, whereas graphite is noble gas free, graphite cannot be the sole diamond precursor. This implies a multiple-stage history. A first generation of diamond could have been synthesized from a noble gas rich precursor or environment by either a shock or a condensation process. Thermally-induced graphitization of chondritic-like organic matter could have produced the graphite, which was then transformed by shock processes into polycrystalline nanodiamond aggregates. The formation of the disordered carbon occurred by diamond post-shock back-transformation during post-shock heating. The noble gases in the first generation diamond could then be incorporated directly into the disordered carbon during the transformation.

1. INTRODUCTION

Ureilites are unique meteorites with a number of intriguing characteristics (Goodrich, 1992; Mittlefehldt et al., 1998; Goodrich et al., 2004, 2007). They are ultramafic

* Corresponding author. Present address: Department of Earth and Planetary Sciences, MSC03-2040, University of New Mexico, Albuquerque, NM 87131-1000, USA. Tel.: +1 505 504 0839.
E-mail addresses: cleguill@unm.edu, corentin.san@gmail.com (C. Le Guillou).

0016-7037/$ - see front matter © 2010 Elsevier Ltd. All rights reserved.
doi:10.1016/j.gca.2010.03.038

rocks generally thought to represent mantle residues, as is evident from their bulk compositions which exhibit depletions in incompatible elements. However, they exhibit thermochemical disequilibrium features and a variable oxygen isotopic composition which, unlike any other achondrite group, fall on a mass-independent fractionation line. One characteristic of ureilites is their high carbon content (from 2 to 6 wt.%; Grady et al., 1985) which occurs as diamond, lonsdaleite (hexagonal diamond), graphite and so-called "amorphous carbon" (Lipschultz, 1964; Frondel and Marvin, 1967; Vdovykin, 1970; Göbel et al., 1978; Grady et al., 1985).

Three ureilite groups can be distinguished: the monomict group, the dimict group and the polymict group. The most recent petrogenetic models suggest that ureilites represent sampling at various depths of the mantle of a heterogeneous parent body which differentiated from a carbon-rich precursor. In a second stage, a shock event disrupted the parent body/bodies and part of the ejected material was re-accreted (Goodrich et al., 2004, 2007; Downes et al., 2008).

To date, carbon in ureilites has been mainly characterized by isotopic studies involving stepped combustion and/or pyrolysis of acid residues (Göbel et al., 1978; Ott et al., 1984, 1985, 1986; Grady et al., 1985; Grady and Pillinger, 1986, 1987, 1988; Russell et al., 1993; Murty et al., 1999; Raï et al., 2003a,b), but combined, multi-scale studies aimed at a complete carbon phases characterization are rare (Nakamuta and Aoki, 2000; Valter et al., 2000; Hezel et al., 2008).

The first association of diamond and lonsdaleite (hexagonal symmetry, space group $P6_3/mmc$, similar to graphite) was discovered in the Canyon Diablo iron meteorite and is ascribed to the solid-state transformation of graphite by dynamic shock-pressure (Heymann et al., 1966; Bundy and Kasper, 1967; Erskine and Nellis, 1992; Langenhorst et al., 1999). In the late 60's, the same association was found in ureilites and was also interpreted as the result of shock (Lipschultz, 1964; Frondel and Marvin, 1967; Valter et al., 2000). The inferred mechanism is a martensitic transition, preserving the morphology of the initial graphite particle. Nevertheless, lonsdaleite can been synthesized experimentally under different conditions: by chemical vapor deposition (CVD; Bhargava et al., 1995), by detonation (Daulton et al., 1996), by shock loading (DeCarli, 1998; DeCarli et al., 2002), by uniaxial pressure on graphite (Yagi and Utsumi, 1992) or from graphite under hydrostatic pressure (Le Guillou et al., 2007) and is thus not a definitive shock indicator. In all these experiments, the nucleation rate of lonsdaleite is very high.

In ureilites, silicate mosaicism is frequent and indicates a shock stage S4 (Stöffler et al., 1991), and the associated pressure range (around 30 GPa) is compatible with the experimental minimum pressure required to produce diamond (Yagi and Utsumi, 1992; Yamada and Tanabe, 2002). Bischoff et al. (1999) established a positive correlation between shock stage and diamond fraction present among carbon material. Grund and Bischoff (1999) observed similar cathodoluminescence properties between terrestrial impact crater diamond and ureilite diamond. All these studies support the shock hypothesis for ureilite diamond formation.

Nevertheless, several cosmochemical characteristics of the carbon species are difficult to explain by shock processes alone and some authors have suggested a nebular condensation origin (such as CVD). First, some weakly shocked ureilites, e.g. Dar al Gani (DAG) 868, do contain diamond (Takeda et al., 2001). Secondly, noble gases are trapped in the diamond with elemental and isotopic compositions similar to "phase Q" or "P1" (Göbel et al., 1978), measured in chondritic insoluble organic matter (IOM) (Huss et al., 1996). This characteristic signature of the IOM of chondrites is acquired before the accretion of the chondritic parent bodies, suggesting a similar origin for ureilite diamond. Among ureilites, Lewis Cliff (LEW) 85328 shows a diamond noble gas concentration exceeding that of Orgueil IOM (Raï et al., 2003b), even though Orgueil is one of the most volatile-rich of all chondrites. It is difficult to understand how shock processing of IOM could produce diamond with noble gas concentrations higher than the precursor. Fukunaga et al. (1987) and then Matsuda et al. (1991, 1995) measured noble gas patterns from condensed and shocked analogues, and argued that the ureilite noble gas pattern was incompatible with shock fractionation, but was reproduced better by condensation.

Finally, Raï et al. (2003a) showed that the N-isotopic composition of diamond, graphite and amorphous carbon could not be explained by formation from a single precursor and also favored a nebular condensation origin.

As far as graphite is concerned, two different formation mechanisms could be invoked. CV chondrites have been proposed as potential precursor materials for ureilites (Goodrich, 2008) and the noble gas compositions between chondrites and ureilites are similar (Göbel et al., 1978). On possibility would then be the thermal graphitization of chondritic organic matter during an internal heating episode (Quirico et al., 2003; Bonal et al., 2006). A second hypothesis is a catalytic graphitization driven by iron, which has been invoked by Berkley and Jones (1982) and is known to be effective experimentally above 1000 °C (Huo et al., 2007; Lian et al., 2008).

The "amorphous carbon" material has been identified by its low combustion temperature (<500 °C) during stepped combustion experiments and has a specific noble gas and nitrogen isotopic signature (Raï et al., 2003a). Raï et al. (2003a) suggested a nebular origin on the basis of its N-isotopic signature, which does not show genetic relation with graphite and diamond. Importantly this phase has never been imaged with scanning electron microscopy (SEM) or transmission electron microscopy (TEM). To our knowledge, no formation mechanisms for this phase have previously been proposed in the literature.

Northwest Africa (NWA) 4742 exhibits unusually large diamond clusters included in an atypical silicate texture, consisting of a combination of pure olivine clasts and "olivine plus pyroxene mosaic matrix". Its oxygen isotopic composition ($\delta^{17}O = 4.71‰$, $\delta^{18}O = 9.61‰$) is extreme and falls on the upper right side of the ureilite trend (Franchi et al., 1997).

Whereas the origin of ureilite diamond has been extensively discussed in the literature, the origin of the other carbon phases and especially of the "amorphous carbon" material, which has never been imaged by TEM, is not constrained. Our approach sheds light on the nanometre scale structure of the various carbon solids and their possible genetic relationships. As diamond is assumed to be linked to shock processing, we compare the features observed in NWA 4742 with laboratory-shocked graphite, partially transformed into diamond. Detailed mechanisms of the shock processes are discussed with a special emphasis given to the "non-diamond" phases.

2. EXPERIMENTAL

2.1. Samples

2.1.1. Northwest Africa 4742

Northwest Africa (NWA) 4742 is a single stone of 376 g found in 2001. One polished section of about 1.5 cm^2 was prepared for scanning electron microscopy and electron microprobe analysis. The presence of millimeter-sized carbon-rich areas bearing diamond prevented satisfactory polishing, resulting in an uneven surface.

A 600 mg piece of the rock was used for chemical separation of the carbonaceous phases and their characterization by XRD, Raman spectrometry and TEM. Some individual smaller fragments of the rock were also used for comparative Raman spectrometry measurements.

2.1.2. Chemical preparation of NWA 4742

About 600 mg of NWA 4742 were provided by the Museum National d'Histoire Naturelle, Paris, France. The sample was crushed in an agate mortar and two residues were prepared. The powdered material was subjected to 4 cycles of HF (12 N)/HCl (1 N), (1:1 vol) and HCl (6 N) treatments. H_3BO_3 (0.9 N) was added in the last two HCl cycles to dissolve secondary fluorides. The aliquot was subsequently rinsed several times in water until pH rose above four and then dried at room temperature (for more details, see Amari et al., 1994). About 20 mg of residue was recovered, i.e. 3% of the original material. This aliquot is hereafter called "HF/HCl residue" and corresponds to the whole insoluble carbon fraction.

Chemical purification was then applied to the "HF/HCl residue" in order to eliminate the non-diamond fraction of the residue. A 9 mg fraction of the "HF/HCl residue" was introduced into a 5 cc Savillex Teflon beaker. Ten successive $HOClO_3$ etches (70%, 160 °C) were necessary to recover a light grey product which was rinsed several times with distilled water and dried at room temperature. This aliquot is hereafter called "PDR" (purified diamond residue).

2.1.3. Laboratory shock-loaded graphite

For comparison with the extracted samples, laboratory-shocked graphite, partially transformed into diamond, was also studied. It was synthesized by Matsuda and coworkers from well crystallized natural graphite by dynamic shock loading at 40 GPa (Matsuda et al., 1995). Shock loading experiments were made using a 25 mm bore single-stage powder propellant gun installed at Tohoku University (Goto and Syono, 1984). Diamond yield is estimated to be between 5% and 15%. These samples have been analyzed by Matsuda et al. (1995) for noble gas content. More experimental details are given in Matsuda et al. (1995).

2.2. Techniques

2.2.1. SEM

We used the scanning electron microscope Zeiss Ultra 55 VP equipped with a field emission gun, at "University Pierre et Marie Curie, Paris, France". The operating conditions were similar to those in Jambon et al. (2005). Beside backscattered electron (BSE) images, energy dispersive spectroscopy (EDS, PGT Sahara) was used to determine the major element composition of the minerals.

2.2.2. Electron microprobe analysis (EMPA)

We used a CAMECA SX 100 microprobe equipped with four WDS detectors in order to obtain analyses of the minerals. Operating conditions were 15 kV accelerating voltage, 10 nA sample current, 10 s counting time and a spot size of 1 μm.

2.2.3. X-ray diffraction (XRD)

X-ray diffraction data were acquired on a DMAX 2500VL Rigaku diffractometer ($\theta - 2\theta$ geometry, vertical goniometer) equipped with a rotating anode (Cu $K\alpha$) operating at 60 kV and 300 mA (graphite back monochromator).

2.2.4. Raman microspectrometry

Raman spectra were collected in the 900–2000 cm^{-1} range with a Raman microspectrometer (Renishaw inVia) using a 20 mW argon laser (514.5 nm, Spectra Physics) and a LEICA (50×) magnification objective (0.5 numerical aperture). To avoid heating of the sample and consecutive shifting of the band position or, worse, structural modification of the material, the laser power on the sample was kept lower than 2 mW.

Diamond has a face-centered cubic crystalline network of C–C bonds, forming tetrahedra. Each carbon atom has four bonds, sp^3 hybridized. The Raman first-order F2g phonon active mode at 1332 cm^{-1} has a full width at half maximum of 1.65 cm^{-1}. Graphite and disordered carbons are mainly composed of sp^2 hybridized atoms forming a Raman active network. The G band at 1580 cm^{-1} is assigned to the E_{2g} vibrational mode (stretching) of the aromatic plane (G). Other bands at about 1200 cm^{-1} (D4), 1350 cm^{-1} (D1), 1620 cm^{-1} (D2) and around 1500 cm^{-1} (D3), called defect bands (D), appear within disordered carbons only (Tuinstra and Köenig, 1970; Wopenka and Pasteris, 1993; Ferrari and Robertson, 2000; Sadezky et al., 2005). We used the areal ratio $R = D1/(G + D1 + D2 + D3 + D4)$ and the full width at half maximum (FWHM-D) of the D1 band to parameterize the relative degree of structural order (Tuinstra and Köenig, 1970; Beyssac et al., 2002; Bonal et al., 2006). With increasing structural organization of the polyaromatic units, R and FWHM

decrease; this corresponds to the progressive loss of the defects, the growth of the polyaromatic units and finally the development of the crystallite size.

We used the WIRE software developed by Renishaw for the spectral fitting procedure. The baseline is a high-degree polynomial adjusted to the observed background shape. The bands are fitted with a combination of Gaussian and Lorentzian functions, the proportion of which is adjusted to each spectrum.

The spectra we report on the following figures are uncorrected raw spectra. The time and number of accumulations is variable among measurements, depending on the response of the different carbon materials.

2.2.5. High-resolution transmission electron microscopy (HRTEM)

We used a JEOL 2011 microscope operating at an acceleration voltage of 200 kV, equipped with an EDS system (PGT system IMIX-PC Si(Li) diode) and a CCD camera (GATAN system ORIUS SC100, 4008×2672 pixels). Magnifications in the range 400–800 kx were necessary to resolve the lattice fringes of graphite ($d_{002} = 0.3354$ nm), disordered carbon ($d_{002} > 0.35$ nm) and diamond ($d_{111} = 0.206$ nm). The sample powders were suspended in alcohol and a droplet was deposited on a lacey carbon film of a Cu TEM grid. All the high-resolution images of disordered carbon were obtained on particles edges located above the holes of the carbon film to avoid confusion between the quasi-amorphous carbon from the supporting film and the carbon from the sample.

3. RESULTS

3.1. Petrologic study

The rock is a monomict breccia (Fig. 1) with abundant olivine clasts (no pyroxenes), several millimeters in size (about 20% of the section surface, as deduced from SEM image analysis), surrounded by a fine-grained matrix (about 75% of the section surface) that contains carbon clusters (about 5% of the section surface).

The clasts (homogeneous composition of $Fa_{21 \pm 2}$) are mosaicized with thin veinlets of iron oxide at subgrain boundaries (Fig. 1), at the scale of about 50 μm. Minor metal, high in Ni and associated with troilite, occurs inside the clasts. On their rims, clasts are invaded by pyroxene introduced at subgrain boundaries, and extending into the clasts for a few tens of micrometers (Fig. 2a).

Outside the clasts, a matrix with small equant crystals (about 50 μm) of both olivine ($Fa_{21 \pm 2}$) and pyroxene is cut by a number of irregular veinlets of sulfide and metal partly converted to oxide (Fig. 2a). Away from the clast rims, interstitial pyroxene (mainly augite, $En_{46}Fs_{12}Wo_{42}$; same Mg# as olivine) around olivine microcrysts is gradu-

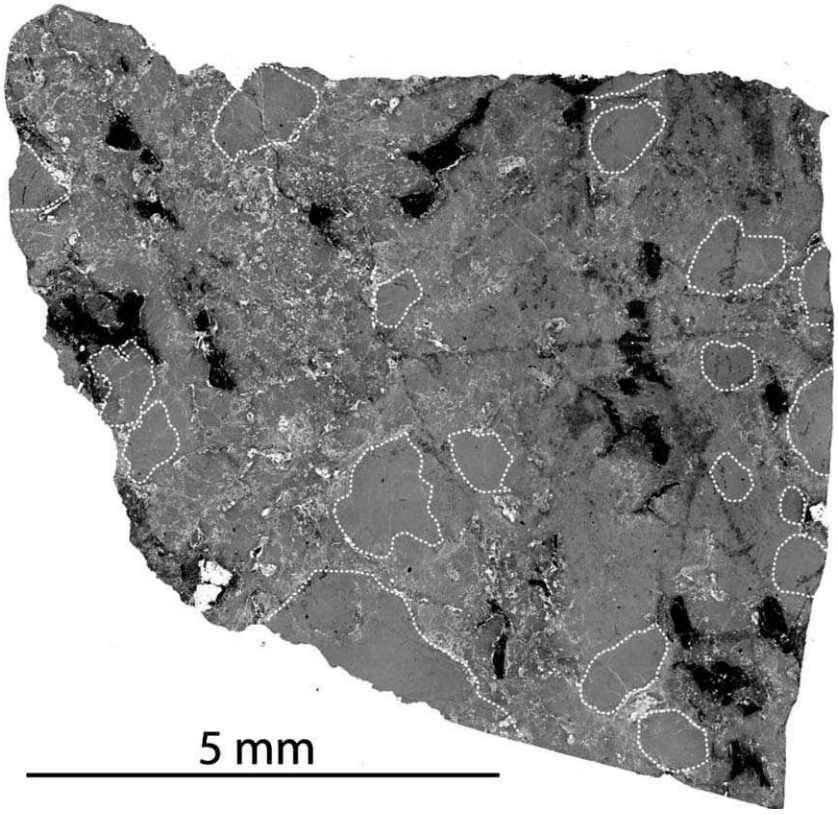

Fig. 1. SEM image (BSE) of the studied polished section of NWA 4742. The white dotted lines circle the olivine clasts (~20%) in order to distinguish them from the mozaicized regions, which dominate the section (~75%). The black areas (~5%) correspond to the carbon clusters. Iron oxide weathering veins are ubiquitous.

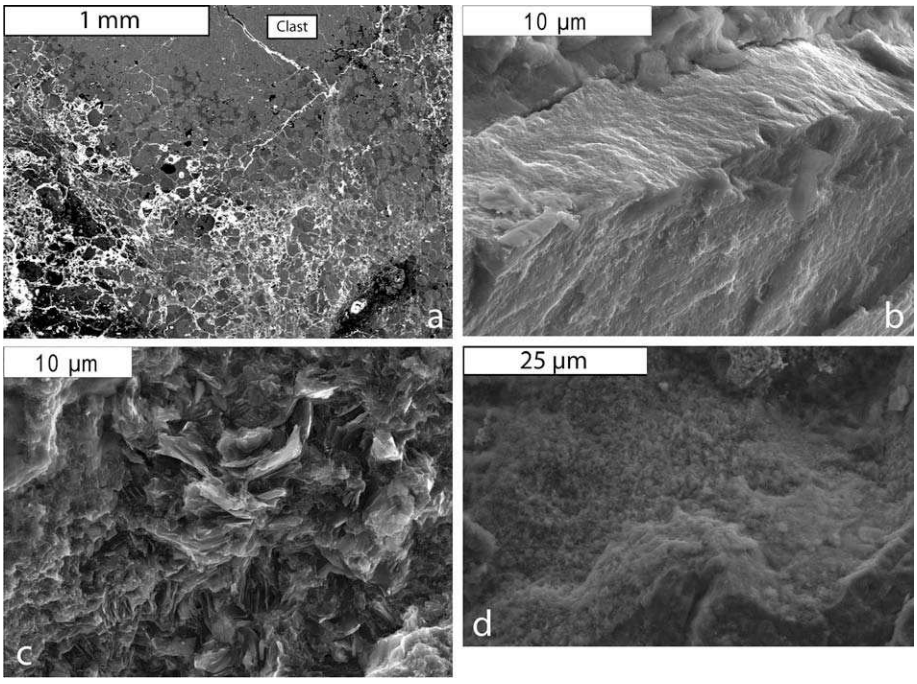

Fig. 2. (a) Close up of Fig. 1 showing the pyroxene (dark grey) intruding the olivine clasts (light grey); (b) SE image of a diamond plate in a raw fragment of NWA4742; (c) SE image of curved graphite particle; (d) carbonaceous crust with nanometric rugosity coating the wall of microfractures.

ally replaced by interstitial olivine around pyroxene microcrysts. The pyroxene Ca content decreases with increasing distance from the clast (from Wo_{42} to Wo_{10}). This texture with regular and equant microcrysts can be termed polycrystalline mosaic. In veinlets in close contact with calcic pyroxene, some rare calcium carbonates appear. They could well be weathering products.

Plagioclase is absent. Within the polycrystalline mosaic, some wide veins mainly filled by carbonaceous materials are observed. The veins exhibit a significant porosity interpreted as the result of fluid circulation, incomplete oxidation of sulfide and metal and the irregular occurrence of large carbon patches (up to several millimeters) connected to one another by a fine array of thin veins (Fig. 1). The reduction of olivine is revealed by its increasing Fo content at the rims of the clasts. Reduction is not limited to clast rims as it also affects olivine microcrysts in the polycrystalline mosaic, where the most Mg-rich olivine is present (up to Fo_{96}). Some less pronounced reduction occurs as well in low-Ca pyroxene. In the reduced areas, metal grains with low Ni content are found, in contrast with the metal from the olivine clasts with high Ni contents.

To summarize, NWA 4742 differs from typical monomict ureilites by its unusually large carbon clusters and its bimodal texture (clasts and polycrystalline mosaicized matrix). At the scale of a few micrometers various types of textures can be observed: stacked plates with a thickness of about 10 µm broken at right angles at their ends (Fig. 2b), or petal-like aggregated platelets <1 µm in thickness (Fig. 2c) are observed. Sometimes some carbonaceous crust with nanometric rugosity (Fig. 2d) lines the wall of micro fractures.

3.2. X-Ray Diffraction

X-ray diffraction (Fig. 3) data from "HF/HCl residue" indicate the presence of four structural types of carbon: strongly disordered carbon, distorted graphite, cubic nanodiamond and nano-lonsdaleite (Table 1). A broad peak with a maximum corresponding to a d-spacing of 0.360 nm ($2\theta = 24.7°$) and a sharp one, centred at 0.337 nm ($2\theta = 26.4°$), indicate the co-existence of quasi-crystalline graphite together with strongly disordered carbon (graphite

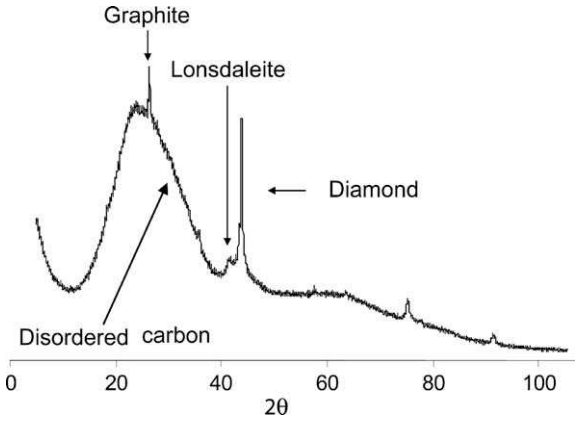

Fig. 3. X-ray diffraction diagram of the "HF/HCl residue". The broad band corresponds to the presence of strongly disordered carbon. A tiny graphite peak ($2\theta = 26.4°$) is superimposed. Nanodiamond and lonsdaleite are identified through their d_{111} (0.206 nm; $2\theta = 43.9°$) and d_{002} (0.218 nm; $2\theta = 41.4°$) peaks.

Table 1
List of the different carbon phases co-existing with diamond in NWA 4742.

	d_{002} (nm)	FWHM-D (cm^{-1})	R (range)	Comment
Graphite	0.335	Band absent	0	Rare
Distorted-graphite	0.337	~58	0.05–0.5	Graphite 0 0 2 planes segmented and ondulated
Disordered carbon	0.36	>100	0.25–0.6	Graphene layers smaller than 10 nm

reference d_{002} value is 0.3354 nm). The presence of compressed graphite ($d_{002} < 0.3354$) has been observed in some ureilites (Nakamuta and Aoki, 2000; Hezel et al., 2008) but was not detected in our sample.

The mean size of coherent diamond domains was estimated using Scherrer's equation. The relation between the size (s, in nm) of the mean coherent domain and the FWHM ($\Delta\theta$ of the peak, in degree) of the 1 1 1 reflection at 0.206 nm ($2\theta = 43.9°$) is expressed by:

$$s = \frac{\lambda}{\Delta\theta \times \cos\theta \times K},$$

where λ is the incident wavelength and K an experimental empirical form factor which is taken equal to 0.9 (Smith, 1989). The experimental width, measured on reference monocrystalline microdiamonds, is first subtracted. This formula yields an average crystalline coherent domain size of 40 nm, whereas SEM images show micrometer-sized particles. This implies that those particles are in fact polycrystalline aggregates of nanodiamonds. Nevertheless, such nanometre size is a lower limit because strain, observed in this sample (see HRTEM Section 3), may also account for part of the diffraction line broadening. However, the coherent domain size inferred by other methods (both Raman spectrometry and TEM, see following sections) is fully compatible with this XRD result.

Lonsdaleite, ($d_{002} = 0.218$ nm, $2\theta = 41.4°$), is revealed by a broad shoulder on the diamond peak ($d_{111} = 0.206$ nm, $2\theta = 43.9°$). Rietveld simulation (Fullprof software, Rodríguez-Carvajal, 2001) has been applied to estimate the relative proportions of crystalline phases (disordered carbons, particularly difficult to integrate, are excluded). The simulation indicates the presence of 85 wt.% diamond, together with 5 wt.% lonsdaleite and 10 wt.% graphite.

The intensity of the disordered carbon peak is high compared to the graphite intensity. Because the diffraction intensity of a non-crystalline material is lower than that of crystalline material, disordered carbon is probably a major component.

3.3. Raman microspectrometry

3.3.1. Purified diamond residue

Raman characterization of diamond on a piece of the ureilite as well as on "HF/HCl residue" powder is difficult for several reasons. First, diamond is embedded within other carbon materials and laser penetration in graphitic material is limited to a few hundred nanometres. At the wavelength of 514.5 nm, the Raman diffusion cross-section of graphitic carbons is at least 60 times higher than that of diamond (Ferrari and Robertson, 2000). In addition, the intensity of Raman diffusion is low because of the small size of the diamond crystallites (~40 nm). For these reasons, the signal of graphitic carbon generally hides the diamond signal.

In order to circumvent this problem, we took an aliquot of the "HF/HCl residue", dissolved the sp^2 graphitic carbon to produce the PDR and measured its Raman spectrum (Fig. 4). The spectra are characterized by: (i) a low intensity (compared to monocrystalline microdiamond), (ii) FWHM between 8 and 27 cm^{-1} (significantly higher than for reference micrometer-sized diamond monocrystals; ~5 cm^{-1}) and a position at 1332 cm^{-1} (close to the diamond reference one, i.e. 1331 cm^{-1}). Fluorescence background is highly variable. Often, no diamond peak can be observed, because it is probably hidden below the fluorescence background.

Literature data on nanodiamonds (<50 nm) indicate, with decreasing size, a progressive Raman shift towards lower wavenumbers (to 1320 cm^{-1} for 5 nm crystallites), an increase of the FWHM and a decrease of the intensity (Yoshikawa et al., 1995; Zhao et al., 1998). In the PDR, the FWHM and the low intensity are consistent with a crystallite size of several tens of nanometres, but the position shift towards lower wavenumbers is not observed. The spectra presented by Miyamoto et al. (1988, 1993) and Karczemska et al. (2008) display the same characteristics. In contrast, Greshake et al. (1999) reported Raman spectra from the ureilite Hammadah Al Hamra 126 with a wide and shifted band (1305 cm^{-1}) that they interpreted as nanodiamonds, possibly mixed with lonsdaleite. These characteristics have also been reported on diamonds from the Ries crater (Lapke et al., 2000). Hezel et al. (2008) reported scattered FWHM with an average value at 7 cm^{-1} but coupled with a slight shift towards low wavenumber, which is not the case in NWA 4742. This difference could originate from internal pressure preserved within diamond aggregates. Indeed, an upshift of the band due to compression (and observed here directly by TEM) could compensate the downshift due to the small grain size (Tan et al., 1998; Zhao et al., 1998; Mermoux et al., 2004).

3.3.2. Polished section and "HF/HCl residue"

The non-diamond carbon fraction of the "HF/HCl residue" shows a wide range of carbon structural order/disorder that can be investigated by comparing several spectral parameters: the D band width (FWHM-D) and the D band area relative to the sum of all other band areas, as described in the experimental section (Tuinstra and Köenig, 1970; Wopenka and Pasteris, 1993; Beyssac et al., 2002; Bonal et al., 2006).

All measurements performed on "rock fragments" indicate a close association of disordered carbon, distorted graphite and diamond within the same carbon veins.

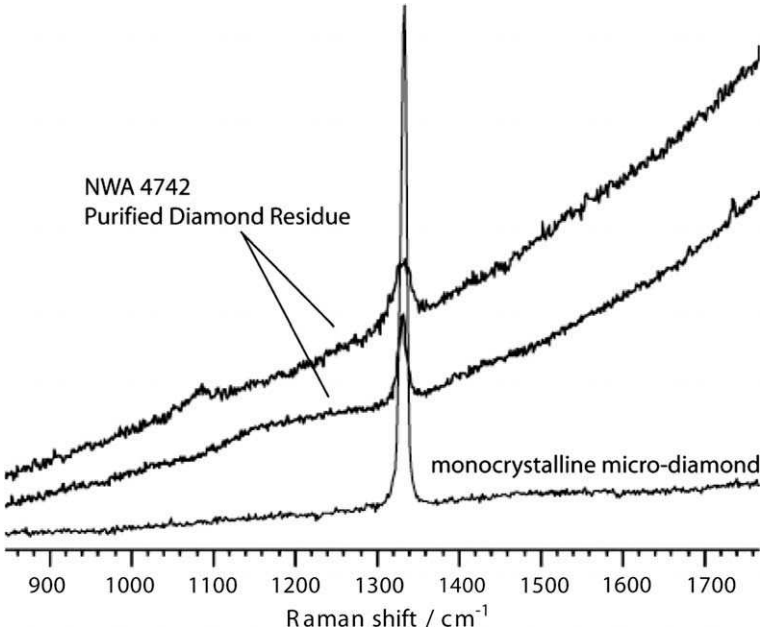

Fig. 4. Raman spectra obtained on the "purified diamond residue" and compared to monocrystalline diamond for reference. The diamond band at 1331 cm^{-1} is very small and has a broad and variable Full Width at Half Maximum. Intense Raman signal, typical of microdiamond, is not observed.

As far as the non-diamond carbons are concerned, two main different structural types are present, which mainly differ in their FWHM-D. Table 1 presents their principal characteristics. Typical spectra are shown on Fig. 5 and are clearly distinguishable. Fig. 6 is a plot of FWHM-D vs *R* ratio. The first group (called distorted graphite hereafter) has FWHM-D values ranging from 40 to 70 cm^{-1} with average at 58 cm^{-1}. The other one (called disordered carbon) has its FWHM-D value widely scattered but always above 100 cm^{-1}. Both groups have variable *R* ratios.

The *R* ratio of the distorted graphite spectra varies between 0.05 and 0.5 with a mean value at 0.4. The scattering of the *R* ratio within this group is too large to be explained by a random orientation of the grains relative to the laser beam (Tan et al., 2001). Consequently, at least a component of the observed scattering may come from a variable degree of disorder of the graphite. This heterogeneity has also been reported by Kagi et al. (1991) from a Raman study of four Antarctic ureilites.

Apart from distorted graphite, highly disordered carbon (Fig. 5) has also been observed. Its Raman parameters are widely scattered (Fig. 6). The main features are a wide defect band (>100 cm^{-1}), a *R* ratio ranging from 0.25 to 0.60 and a broad E_{2g} mode upshifted in position by

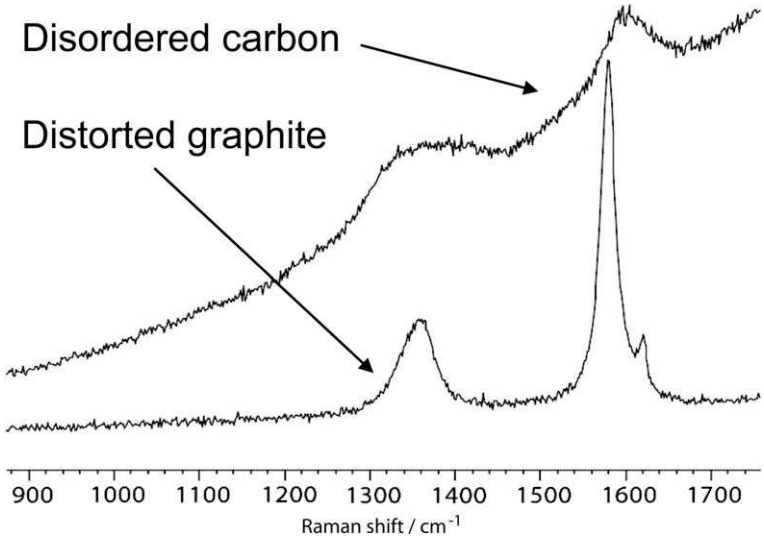

Fig. 5. Two typical Raman spectra measured *in situ* within the same carbon cluster on "raw rock fragment" (*i.e.* chemically untreated). All phases are present. However, diamond signal is hidden by graphitic carbon signal. The upper spectrum is typical of the "disordered carbon group", the lower of the "distorted graphite group". These spectra are also measured on the "HF/HCl residue".

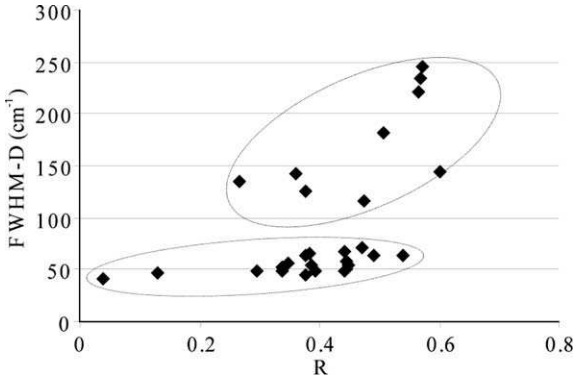

Fig. 6. Raman spectral parameters measured on the "HF/HCl residue": Full Width at Half Maximum versus relative surface ratio of the defect band with respect to the other bands. Two different groups of carbons are identified which do not show structural continuum.

20 cm^{-1}. These features correspond to strongly disordered carbons with nanometre-sized polyaromatic layers, as revealed by the HRTEM images (see below). Nevertheless, they represent a population clearly distinguishable from the distorted graphite population.

Rare spectra also reveal broad bands around 1120 and 1500 cm^{-1}, both characteristic of short-range carbon organization (Fig. 7a). The 1500 cm^{-1} band could be attributed to strictly amorphous carbon composed of a mixture of sp^2 and sp^3 bonds, without aromatic structure (Bény-Bassez and Rouzaud, 1985; Sadezky et al., 2005). The 1100–1150 cm^{-1} band assignment still remains unclear. Isolated sp^3 carbon tetrahedron as well as sp^3 hydrogenated nanodiamond surface bonds have been invoked to explain this feature in the literature (Shröder et al., 1990; Ferrari and Robertson, 2001; Michaelson et al., 2006). These bands are also reported in Le Guillou et al. (2007) from materials composed of intermixed diamond and disordered carbons.

Some spectra, recorded on fragments of the "HF/HCL residue", as well as on PDR, are "signal depleted" or "Raman inactive" (Fig. 7b), whereas fluorescence is absent. A similar feature has been previously described by El Goresy et al. (2001, 2003) on carbons from shocked gneiss of the Ries crater, Germany. They observe the same association of diamonds, graphite and disordered carbon. They measured the "Raman inactive" phase with X-ray synchrotron facilities, and assigned this signal to a "new", transparent, ultra-hard carbon phase.

3.3.3. Laboratory shock-synthesized diamond

In order to understand the various Raman features described above, we performed measurements on the laboratory-shocked graphite. Only the sp^2 fraction could be characterized because the diamond was not abundant enough to be detected with the 514.5 nm wavelength used.

The starting material (not shown), is natural graphite and only shows a G band. Fig. 8a displays two different spectra measured on the experimentally shocked graphite. They show a significant contribution from the D_1 band and are heterogeneous. To quantify these heterogeneities, more than 20 spectra have been fitted. As for NWA 4742, four or five bands were used (~1200, 1350, ~1500, 1580 and 1620 cm^{-1}). Fig. 8b shows the relation between the

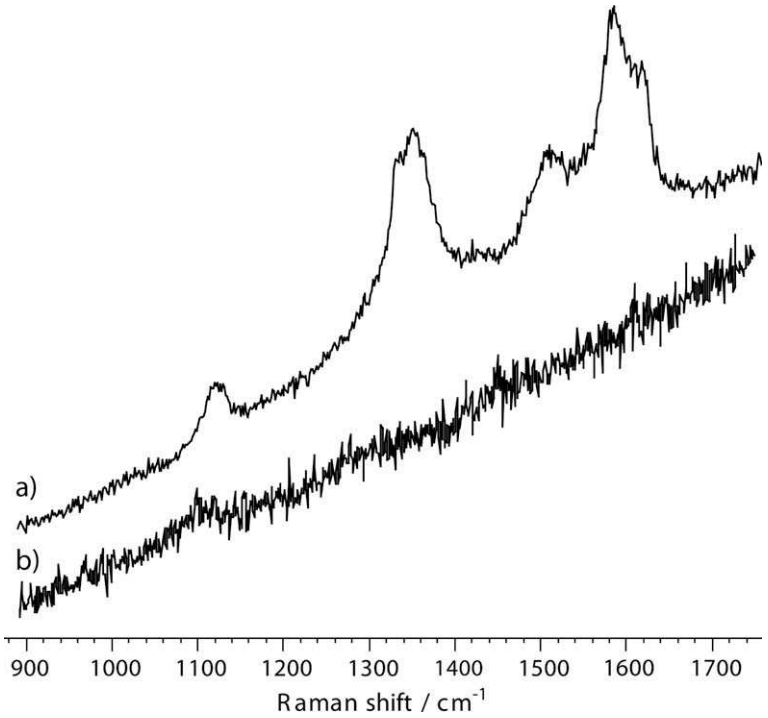

Fig. 7. Two exotic spectra. One (a) has the 1120 and 1500 cm^{-1} bands related to hydrogenated and/or almost amorphous materials and is measured on the "HF/HCl residue". The other one (b) is featureless, has no fluorescence background and is obtained on the "purified diamond residue".

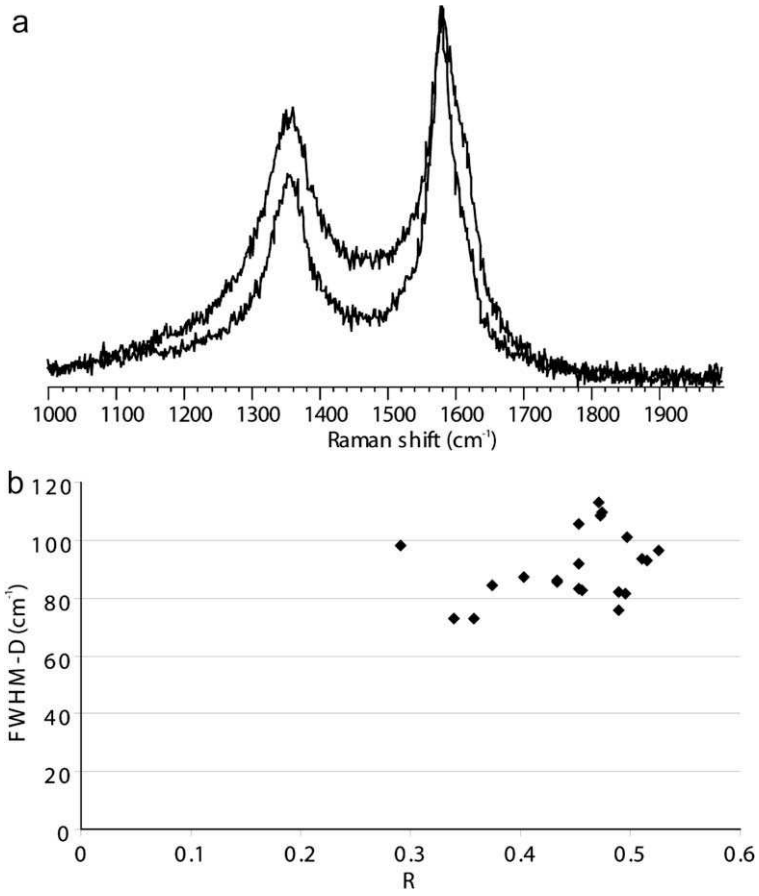

Fig. 8. (a) Typical Raman spectra measured on the experimentally shocked graphite powder partially transformed into diamond. The intensity of the spectra is normalized to the G band intensity. It shows the presence of contributions at 1200, 1350, 1500, 1580 and 1620 cm^{-1}; (b) Raman parameters extracted from the measured spectra. The variability of the FWHM-D and of the *R* ratio is significant.

FWHM of the D band and the *R* ratio. The scattering of the *R* (between 0.3 and 0.5) and FWHM (between 73 and 113 cm^{-1}) values illustrates the structural heterogeneity of the sample, and demonstrates that a single shock on a homogeneous precursor can produce structural variability. As in NWA 4742, several measurements display similar FWHM (~80 cm^{-1}, higher than in NWA 4742) with variable *R* ratios. However, the laboratory-shocked sample only displays one population whereas NWA 4742 displays both 'disordered carbon' and 'distorted graphite' groups. These discrepancies could arise from the difference in pressure-temperature conditions and especially from the different cooling rate between experimental and NWA 4742 samples.

3.4. High-resolution transmission electron microscopy

3.4.1. Purified diamond residue

Dark-field TEM enables direct imaging of the coherent diamond domains. Scanning electron microscopy shows

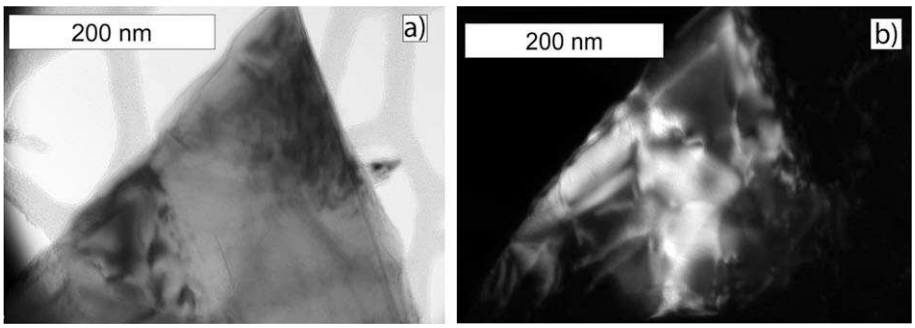

Fig. 9. Bright-field (a) and dark-field (b) TEM image of a particle from the "separated diamond residue". The contrasted zone on the dark-field mode image indicates the polycrystallinity of the particles. Domain sizes (~50 nm) are consistent with XRD analysis.

only single diamond particles of various sizes, but dark-field TEM can help to refine the structural characteristics of the particles and especially to distinguish polycrystalline nanodiamonds from monocrystals.

Fig. 9a shows a bright-field image of a 400 nm large particle. In the corresponding dark-field image (Fig. 9b), the objective aperture was centred on a position where only the periodicity corresponding to a d-spacing of 0.115 nm contribute to the image. This periodicity has been identified as the 109 reflection of lonsdaleite (Ownby et al., 1992). The main information from this technique is that the whole grain does not diffract as a single coherent crystal. Whereas the particle shows sharp edges in bright-field mode, which may suggest a monocrystal, the dark-field images demonstrate that this grain is in fact an aggregate of individual domains.

This result has to be interpreted carefully; dark-field images cannot be obtained from the largest particles as they are too thick to be transparent to the electrons. However, the good agreement of TEM data with XRD and Raman measurements excludes the presence of dominant micrometric single crystals of diamond in NWA 4742.

To summarize, dark-field TEM images of diamonds (both cubic and hexagonal) demonstrate the systematic presence of polycrystalline aggregates, independent of the particle size, with coherent domains several tens of nanometres in size.

Using HRTEM, the smallest observed isolated diamonds display crystallite sizes of a few nanometres, the largest ones are smaller than 100 nm.

Fig. 10 illustrates the presence of frequently observed Bragg fringes in diamond, which are the result of slight lattice distortion. This feature results from interference errors depending on the reciprocal node length and relates to the coherent domain size. In this case (about 40 nm coherent domains), such fringes correspond to deformation angles of about 1°.

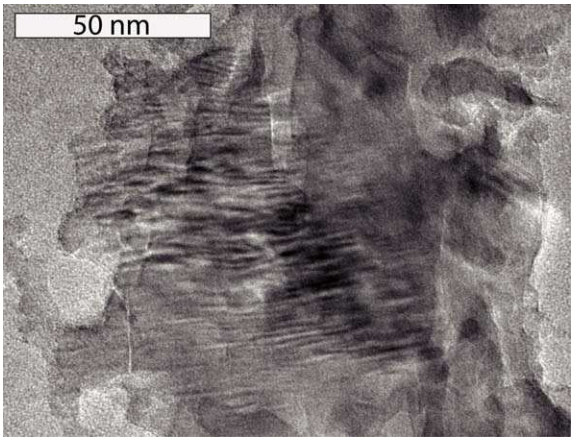

Fig. 10. TEM image of a diamond particle from the "purified diamond residue" showing Bragg fringes. The latter are interpreted as due to lattice strain.

3.4.2. HF/HCl residue

Crystalline graphite (Fig. 11a), distorted graphite, and disordered carbons associated with nanodiamonds

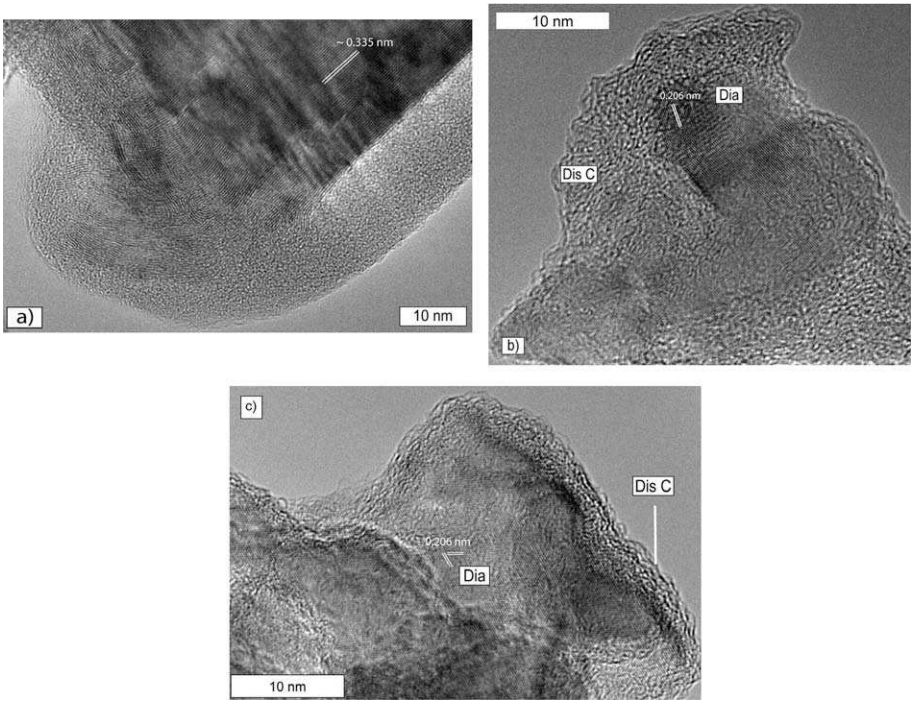

Fig. 11. High-resolution TEM images from the "HF/HCl residue". Edge of a graphite particle ($d_{002} = 0.335$ nm) (a), nanodiamond (*Dia*, $d_{111} = 0.206$ nm) embedded within strongly disordered carbon (*Dis C*) (b), and nanodiamond surrounded by disordered carbon showing nanometre size fringes parallel to the grain surface (c). In both cases, disordered carbon and diamond are intimately related.

(Fig. 11b and c) are observed in the residue. As a complement to the "purified diamond residue" observations, the relations between diamonds and other carbon phases were investigated. Diamond aggregates appear frequently embedded within weakly organized turbostratic carbons at the nanometre scale (Fig. 11b and c).

The disordered carbon seems to present a structural continuum between amorphous-like carbon (mixture of sp^2 and sp^3 bonds, responsible for the absence of periodic organization of carbon atoms) and small polyaromatic units, better organized at the nanometre scale, but still strongly disordered (largest polyaromatic layers limited to a few nanometres). This organization degree observed by TEM is compatible with the Raman spectra showing the highest FWHM-D.

Nanodiamonds sometimes occur in a disordered carbon matrix. The 0 0 2 fringes of the disordered carbon show no specific orientation relative to the diamond 1 1 1 fringes in Fig. 11b. Nevertheless, most of the time, polyaromatic layers are mostly parallel to the diamond grains surface (Fig. 11c), suggesting that there is a crystallographic orientation relationship between the atomic planes of these two carbon phases, i.e. a topotaxial growth. The number of stacked layers of the disordered carbon phase is variable, but never exceeds 10.

The degree of organization of this disordered carbon is variable. Fig. 11b illustrates an extreme situation where a single diamond crystallite is surrounded by a nearly amorphous carbon, which presents no noticeable geometric relationship with diamond. This material is not limited to a surface layer but completely surrounds the nanodiamond on a larger scale (~10–20 nm). These strongly disordered structures have also been reported by Langenhorst et al. (1999) together with diamond-graphite mixtures in the Popigaï impact crater.

One interesting observation is reported in Fig. 12. It consists of a micrometer-sized particle made of diamonds included in distorted graphite (Fig. 12a). The electron diffraction pattern of this grain shows two small arcs corresponding to periodicities at about 0.35 nm (due to distorted graphite 0 0 2 planes) and two spots at 0.206 nm (due to the diamond 1 1 1 planes) oriented along the same direction. These two families of planes are the closest-packed atomic planes of graphite and diamond, respectively, and show parallel orientation. The crystallographic relationship is shown in detail in Fig. 12b (lattice-fringe mode). The latter shows the relationship between diamond (right side) and distorted graphite (left side). In contrast with our other observations, diamonds here are not coated by disordered carbon (Fig. 12c). In this case, the diamond is included in an organized structure. Furthermore, the polyaromatic units are located only along the 1 1 1 diamond planes (Fig. 12b) and do not entirely surround the crystal (Fig. 12c), a relationship which has been observed for ther-

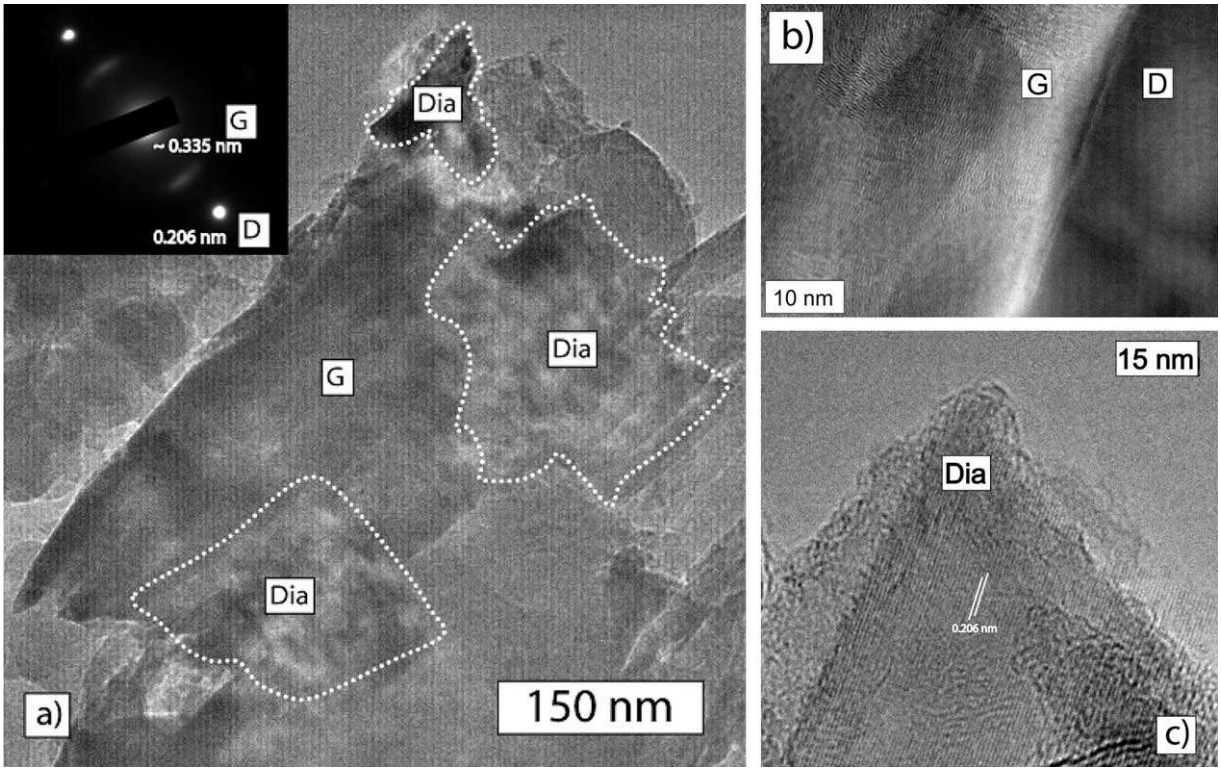

Fig. 12. Particle from the "HF/HCl residue". Diamonds (circled in white) are included in distorted graphite (G, $d_{002} = 0.335$ nm) (a). The selected-area electron diffraction pattern demonstrates the parallelism between diamond 1 1 1 planes and distorted graphite 0 0 2 planes. The latter are not perfectly structured as indicated by the presence of a diffraction arcs rather than a spot. Enlargements of two specific regions are shown: boundary between diamond and distorted graphite (b), and diamond located on the extremity of the particle (c) and showing that distorted graphite does not fully surround diamond.

mal graphitization of diamond (Butenko et al., 2000). Collectively this evidence clearly indicates the formation of diamond directly from graphite. Similar inclusion of diamond into graphite particles have been reported from the Novo Urei ureilite (Valter et al., 2000).

Almost crystalline grains of graphite are observed (Fig. 11a) but HRTEM also reveals distorted structure (Fig. 12b). The polyaromatic layers are wrinkled along the whole grain, and frequently disrupted. The distorted graphite population is, at the TEM observation scale, structurally heterogeneous and correspond to the group of Raman spectra having a mean FHWM value of $\sim 58\ cm^{-1}$ and scattered R ratio.

3.4.3. Laboratory shock-synthesized diamonds

Our HRTEM study reveals various carbon structures at the nanometre scale. Some are similar to those found in NWA 4742 carbon residue, and some differ. Unmodified crystalline graphite (Fig. 13a), distorted graphite (Fig. 13b), strongly disordered carbon together with nanodiamond (Fig. 13c) and carbon-coated diamonds (Fig. 13d) look similar to NWA 4742 material. As expected for a short time scale dynamic experiment, no growth occurs and the typical size of the diamond coherent domains is limited and comparable to that of NWA 4742, i.e. between 10 and 100 nm, approximately.

Some differences are observed, however. First, the diamond crystallites are not polycrystalline nor aggregated, but occur as individual crystals. Diamond inclusions within graphite were not observed. These two features may result from a lower shock degree in the experiment. Furthermore, the extent of material coating nanodiamonds is far larger than around NWA 4742 diamond.

Fig. 14 shows a diamond core surrounded by sp^2 "onion-like" structure. This nanostructure is typical of annealed nanodiamonds (Butenko et al., 2000), transformed into concentric particles rather than into lamellar ones

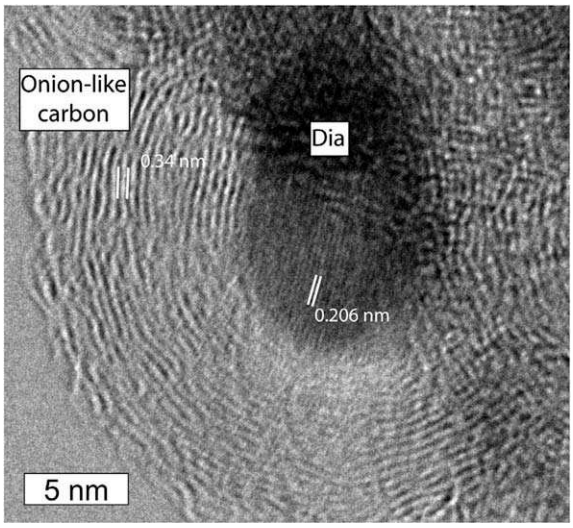

Fig. 14. High-resolution images from the shocked graphite sample partially transformed into diamond. Diamond core (1 1 1 planes are apparent) coated by continuous 0 0 2 carbon layers interpreted as the partial back-transformation of nanodiamonds formed during the shock.

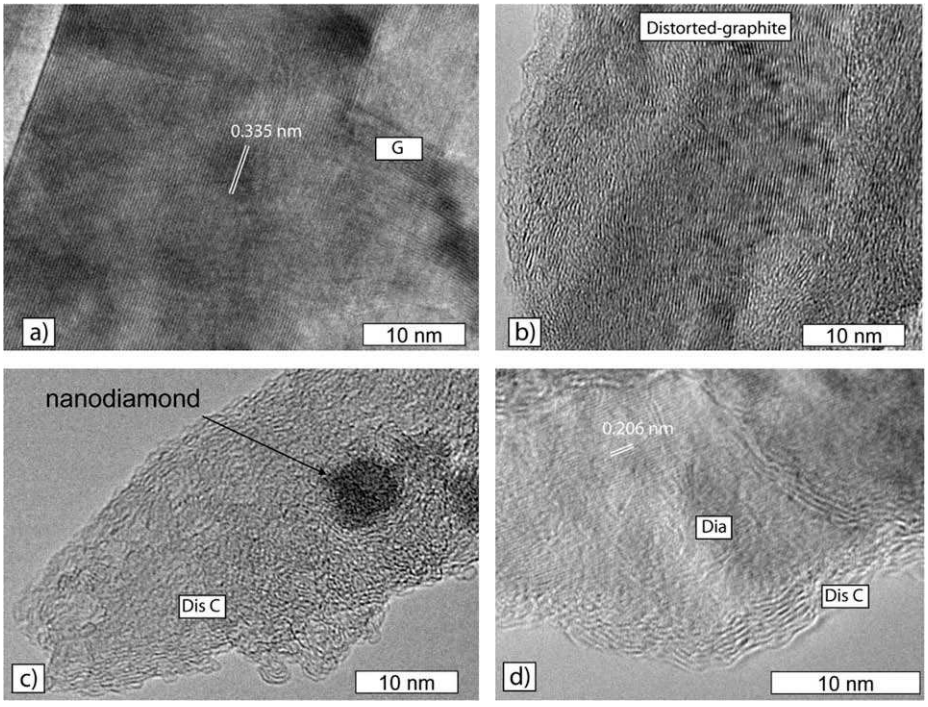

Fig. 13. High-resolution TEM images from the shocked graphite sample partially transformed into diamond. (a) Original graphite, (b) distorted graphite, (c) nanodiamond located in the middle of a strongly disordered carbon, and (d) nanodiamond (*Dia*) particle showing distorted 0 0 2 graphene fringes (*Dis C*) parallel to the grain surface.

because of the nanodiamond critical size. Such rims are usually interpreted as post-shock thermally back-transformed nanodiamonds (Morris, 1980; Butenko et al., 2000).

The main characteristic shock features observed in the laboratory-shocked graphite are the preservation of some graphite grains, the decrease of the ordering of other grains (undulations, breaking of the graphene plane, partial amorphization), a small diamond crystallite size and coatings on the diamonds.

4. DISCUSSION

In the first part, we discuss the crystallographic structure of diamonds in the ureilite NWA4742 and the nature of its precursor (graphite rather than disordered organic matter). Then, the degree of structural ordering of the distorted graphite and the associations of diamond with disordered carbon are compared to laboratory shock experiments. These data are critical to understanding the relationships between disordered carbon, distorted graphite and diamond, and to better constrain the noble gas reservoirs in ureilites. We propose a scenario for genesis and evolution of NWA 4742 carbon components, based on their crystallographic phase relations.

4.1. Diamond precursor and structure

TEM suggests that at least some polycrystalline aggregates of nanodiamond and lonsdaleite (average coherent domain size of about 40 nm) in NWA 4742 were formed by shock through a solid-state transformation of graphite. A CVD origin, although not completely ruled out, cannot be the sole formation mechanism.

4.1.1. Diamond originating from graphite

The particle in Fig. 12 shows that graphite is the precursor for (at least) some diamonds. This particle is made of diamonds included within distorted graphite (Fig. 12a) and their respective closest-packed planes (1 1 1 for diamond and 0 0 2 for graphite) show parallel orientations (Fig. 12a and b). Such a particle has also been reported from the Novo Urei ureilite (Valter et al., 2000). At this point, there are two possibilities to explain this association: the formation of diamond from graphite or the formation of graphite from previously formed diamonds.

Literature data (Butenko et al., 2000; Le Guillou et al., 2009), together with our experimental work (Fig. 14), show that graphitization of diamond produces continuous surface layers of graphene around diamond grains. In NWA 4742, the distorted graphite is made of graphene layers which: (i) do not entirely coat the diamond crystals, (ii) are present only along the 1 1 1 diamond planes. These observations favor a direct, but incomplete, transformation of graphite into diamond, likely by a shock-induced martensitic mechanism (Morris, 1980; Yagi and Utsumi, 1992). This mechanism minimizes the atomic displacements and thus preserves the morphology of the graphite precursor particle. It is also known to yield lonsdaleite (observed in NWA 4742) in addition to cubic diamond. In this case, the distorted graphite is not the result of diamond graphitization (secondary graphite) but rather the distorted remnants of the graphite precursor.

Another argument for the graphite to diamond transformation relies on the work of El Goresy et al. (2001). They described a super-hard carbon phase from the Ries crater gneiss which was "Raman inactive" and was, along with lonsdaleite, attributed to the shock transformation of graphite. We also detected "Raman inactive" particles in our purified diamond residue, showing no fluorescence and no Raman contribution (Fig. 7b). This similarity supports the shock origin.

4.1.2. Crystal size, aggregation, deformation and lonsdaleite

Based on XRD and dark field mode TEM imaging, we demonstrate that diamonds in NWA 4742 are polycrystalline aggregates rather than monocrystals. The size of the aggregates can be micrometers (Fig. 2b), but the coherent monocrystalline domains are smaller than 100 nm, with an average size deduced from XRD of about 40 nm. Bragg fringes, originating from slightly strained crystal lattices, are frequently observed. Pressure is required to account for this deformation and is also known to produce polycrystalline diamonds of nanometre size, as well as lonsdaleite (He et al., 2002). The latter has a hexagonal symmetry (space group $P6_3/mmc$) similar to graphite. Those minerals are crystallographically anisotropic in contrast to cubic diamond.

In the last 20 years, various techniques based on "isotropic" formation conditions have been elaborated for diamond synthesis such as: Chemical Vapour Deposition with various methods and substrates (Setaka, 1987, 1989; Frenklach et al., 1989, 1991; Bachmann et al., 1991; De Barros and Vandenbulcke, 2000; Vandenbulcke et al., 2009), electron irradiation of carbon onions (Banhart, 1997), CH_4 dissociation at high pressure (Benedetti et al., 1999) or decomposition of silicon carbides (Gogotsi et al., 2001). As far as the mechanical constraints are concerned, those synthesis methods are all "isotropic" and produce cubic diamond rather than lonsdaleite, which is not observed in these experiments. In contrast, products synthesised by "anisotropic methods" like shock waves in a gas phase or mechanical shock loading on various precursors (DeCarli and Jamieson, 1961; Bundy and Kasper, 1967; Morris, 1980; Erskine and Nellis, 1992; Yamada and Tanabe, 2002) contain lonsdaleite. Anisotropy seems to be a requisite for lonsdaleite synthesis.

However, the synthesis method is not the only control; the precursor anisotropy itself also has to be considered. Under high hydrostatic pressure, the hexagonal diamond polymorph can be produced from graphite (strongly anisotropic), but not from amorphous isotropic carbon (Le Guillou et al., 2007). This is due to the structural anisotropy of the precursor itself. To summarize, every time lonsdaleite is produced, anisotropy must be involved, arising from the precursor or from external forces. In NWA 4742, lonsdaleite obviously results from shock transformation, and condensation mechanisms appear very unlikely.

Some diamond and lonsdaleite crystals in NWA 4742 formed from graphite by shock-induced transformation, but this conclusion is not completely satisfying as it does not explain all the noble gas data obtained on various urei-

lites. Formation of diamond by other mechanisms is certainly required to explain the noble gas data.

First, previous works showed that diamond is the main carrier of noble gases, whereas graphite is almost free of noble gas (Göbel et al., 1978; Raï et al., 2003a,b). It seems impossible to produce "diamond containing noble gases" from a noble gas depleted precursor. Furthermore, Matsuda et al. (1995) demonstrated that isotopic fractionation during transformation of diamond into graphite was unable to explain the actual noble gas signature in ureilite.

To reconcile these apparent contradictions, we suggest the existence of two diamond populations. The first one would contain noble gases. It could be synthesized by shock on a noble gas rich material (possibly on the chondritic-like carbon of the ureilite parent body), or prior to accretion in the solar nebula, for instance by condensation as proposed by Fukunaga et al. (1987). The second population of diamond could be formed by a later shock on graphite.

Interestingly, polycrystalline aggregates of diamond and lonsdaleite can also be formed by shock on already existing (monocrystalline) diamond (He et al., 2002). As the difference between cubic and hexagonal forms simply relies on the stacking sequence (ABC vs AB), lonsdaleite occurs as an intercalated stacking sequence produced by shock on cubic diamond. In our hypothesis, new diamonds are formed from graphite, but a first generation (which would contain noble gases) could also be simultaneously modified. Consequently, a late shock on previously formed diamonds mixed with graphite would explain the observed features: diamond inclusions in distorted graphite, lonsdaleite, polycrystalline diamond aggregates and Bragg fringes.

4.2. Distorted graphite, structure and origin

CV chondrites have already been considered as potential precursors for ureilite material as a whole (Goodrich, 2008). In chondrites, insoluble organic matter is the main carbon component and has a noble gas composition close to ureilite carbon phases (Göbel et al., 1978). Thus, graphite itself may result from the sluggish thermal graphitization process of organic matter, during asteroidal metamorphism, with or without the help of a metal catalyst (Berkley and Jones, 1982). These mechanisms are studied extensively in terrestrial rocks (maturation and graphitization during diagenesis and metamorphism; Jehlicka and Rouzaud, 1990; Oh et al., 1991; Wopenka and Pasteris, 1993; Beyssac et al., 2002) and experimental materials (Huo et al., 2007; Lian et al., 2008) and can thus be evaluated.

Presolar graphites have been reported in chondrites (Croat et al., 2004) and were probably formed by condensation but they are not a significant carbon source and will not be considered.

In NWA 4742, we observe a population of distorted graphite with structural heterogeneities, from well crystallised graphite to more or less distorted crystals. The abundance of this material is quite low compared to diamond (~10 wt.%) as deduced from XRD Rietveld analysis.

Scattering of the R Raman ratio between 0.05 and 0.55 is significant (Fig. 6, first group, FWHM ~58 cm^{-1}) but the FWHM is constant within this carbon population. Structural variability of carbon has already been reported by Kagi et al. (1991) in four Antarctic ureilites (Raman spectrometry study) and by Smith et al. (2001) from stepped combustion experiments. The latter interpreted the broad temperature range of combustion to variable carbon structures in the sample. Our detailed characterization by Raman and HRTEM enables an improved understanding of those features.

As temperature increases, the carbon structural organization progressively and irreversibly improves (growth and stacking improvement of the graphene planes, occurrence of tri-periodic order). In terrestrial rocks (Jehlicka and Rouzaud, 1990; Oh et al., 1991; Wopenka and Pasteris, 1993; Beyssac et al., 2002), as well as in chondrites of different metamorphic grades (Quirico et al., 2003; Bonal et al., 2006, 2007), progressive re-organization of organic matter leads to a decrease of the R ratio, but this evolution occurs together with a decrease of the FWHM of the D band. The type of heterogeneity we observe here is unlikely to be due to such processes. In contrast, and as shown by the Raman spectral analysis of the shock experiment, heterogeneous "loss of crystallinity" of graphite occurs during a single shock event. Shock can then be a simple mechanism that explains both the Raman and HRTEM observations in NWA 4742.

If the heterogeneity of the distorted graphite really arises from shock effect, the degree of structural organization of the carbon material before the shock should be indicated by the lowest R ratio ($R \sim 0.1$), which corresponds to almost crystalline graphite with limited grain size (smaller than the Raman beam size). About 600 °C is necessary in metamorphic terrestrial rocks to reach this graphitization stage (Beyssac et al., 2002). As timescales of terrestrial and asteroidal parent body metamorphism are similar, this temperature estimation is reliable. Indeed, the timescale of asteroidal metamorphism is mostly controlled by the ^{26}Al decay, whose half-life is ~7.10^5 years, and models predict that the metamorphic peak should last ~1 My for a small asteroid (radius ~20 km) up to ~100 My for a 200 km radius asteroid (Bennett and McSween, 1996). Consequently, graphitization could be achieved at temperature lower than silicate partial melting temperatures, and short-timescale (shock-melting for instance) metal-induced catalytic graphitization, although possible, is not required. In a recent petrogenetic model of ureilites, Goodrich et al. (2004) consider that disruption of the parent body by the shock event occurs while the asteroid, in the course of differentiation (internal heating), is still hot. In this scenario, graphitization of organic matter would be achieved prior to the shock that caused breakup of the ureilite parent body. The presence of primitive chondritic organic matter as a precursor for graphite is thus consistent with this hypothesis.

The thermal expansion of graphite is one order of magnitude higher than that of diamond. This property could explain why graphite has lost its noble gases during metamorphic events. In contrast, if an early diamond generation was present, it could have retained its noble gases.

4.3. Association of diamond with disordered carbon

If graphite is the product of thermal transformation of organic matter remnants of disordered carbon should have disappeared. Consequently, the formation episode of disordered carbon in NWA 4742 must postdate this thermal event.

One of our main results is that the component which was previously called "amorphous carbon" in the literature, and whose nature was unknown until now, has now been imaged directly by TEM. It is renamed here disordered carbon since such carbons are never *stricto sensu* amorphous, because they systematically show nanometre-sized polyaromatic structures. A good agreement exists between the HRTEM observations and the Raman spectra of the "disordered carbon group". This material is intimately and systematically associated with diamonds. As discussed earlier, this material coats the diamond and aromatic layers are often oriented parallel to the grain surface (Fig. 11c), indicating a topotaxial growth.

Two possibilities exist to explain the disordered carbon association with diamond: (1) partial graphitization of diamond by extended heating, (2) destabilization of diamond by post-shock annealing.

4.3.1. Solid-state partial graphitization of diamond by internal heating?

Diamond is not stable at low pressure and would be expected to undergo graphitization during internal heating of the parent body and for timescales corresponding to ^{26}Al decay.

Experimental results (Butenko et al., 2000) have shown that graphitized diamond displays continuous, aromatic layers coating the external part of the diamond. In our sample, this characteristic is not generally observed. Instead, coating layers are discontinuous around the diamond and show structural variability, from almost amorphous material to imperfectly stacked layers of 1–2 nm length. Raman spectra further confirm this heterogeneity through the FWHM scattering of the defect band. A long internal heating episode is thus unlikely to explain the association of diamond and disordered carbon in NWA4742.

4.3.2. Post-shock annealing and comparison to laboratory analogues

In contrast, coating structures are observed in the laboratory-shocked analogues (Fig. 13d), where short graphene layers surround the diamond. During a shock, the thermal wave propagates more slowly than the mechanical wave. Depending on the material and the shock-pressure conditions, the associated temperature induces more or less back-transformation of diamond (Morris, 1980; Erskine and Nellis, 1992). These disordered structures have already been reported by Langenhorst et al. (1999) together with diamond-graphite mixtures in the Popigaï impact crater. When nanodiamonds are completely back-transformed to graphitic material, they form onion-like structures as illustrated in Fig. 14. The various observed structures and transformation degrees are attributed to material and shock wave propagation heterogeneities, which yield heterogeneous heat dissipation and diamond transformation rates.

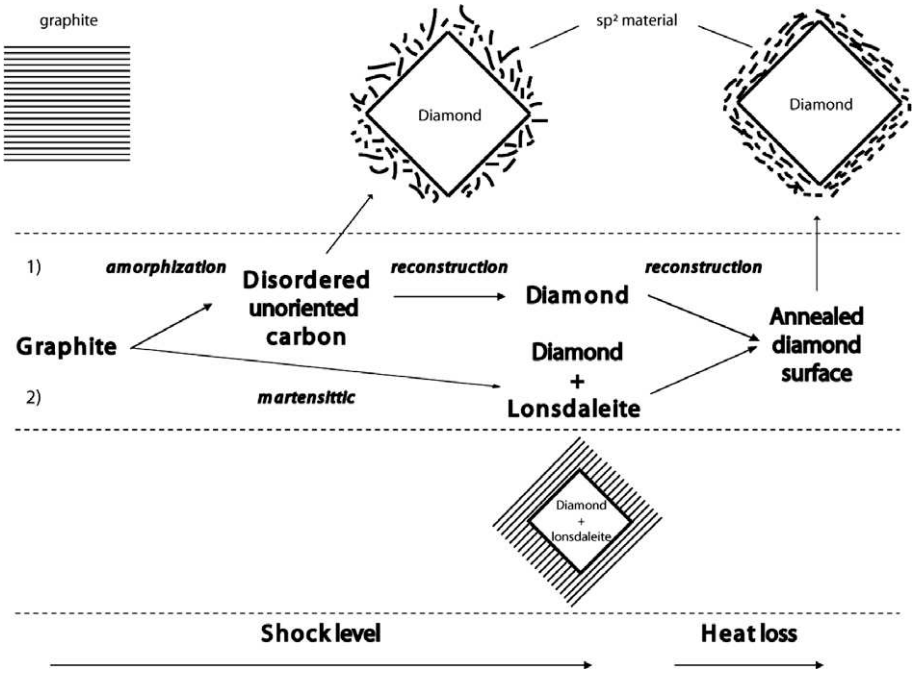

Fig. 15. Schematic diagram summarizing the various mechanistic paths of the solid-state transformation of graphite to diamond as deduced from literature data and from our Raman and TEM observations. Path 1 implies that at least partial amorphization of the graphite precursor is necessary to reconstruct cubic diamond. An intermediate situation leads to nanodiamonds included in strongly disordered carbon. Path 2 represents the martensitic transition from graphite to lonsdaleite and/or diamond. Both paths yield a sp^2 coating on the diamond surface, formed during post-shock annealing.

Heterogeneous redox conditions within the sample during the shock could also be invoked.

Fig. 15 is a tentative sketch representing the different paths of diamond formation occurring during shock events, based on literature data and on our TEM observations of experimental products. Graphite can be directly transformed into diamond (cubic and/or hexagonal) by a martensitic transformation mechanism (Morris, 1980; Erskine and Nellis, 1992; Yagi and Utsumi, 1992), but this mechanism (path 2) alone cannot explain all the observations. Another mechanism also has to be considered where graphite could first lose its crystallinity to various degrees (path 1) as a transitional step in the transformation to diamond.

Indeed, experimental and NWA 4742 samples show diamonds embedded within strongly disordered carbon whose graphene layers are not parallel to the diamond surface (cf. Figs. 13c and 11b). This situation can be interpreted as an incomplete transformation of graphite into diamond and corresponds to path 1 in Fig. 15. In this case, partial amorphization would be a pre-requisite for cubic diamond nucleation (Yamada et al., 1999; Yamada and Tanabe, 2002) as also suggested for static high-pressure conversion of graphite into diamonds (Onodera and Irie, 1991; Le Guillou et al., 2007). This transformation mechanism is reconstructive.

This transformation pathway could be comparable to the high pressure experiments of Mao et al. (2003), where an intermediate phase is revealed in the course of the transformation of graphite into diamond. To obtain this intermediate phase, some of the sp^2 bonds are changed into sp^3 bonds while the graphite crystallographic structure is preserved. Such an unstable intermediate structure, if attained during the impact event, could yield strongly disordered carbon after the release of the shock stress.

Depending on the shock conditions, the two transformation paths could occur. In NWA 4742, the observations favor a combination of the two mechanisms. In every case, disordered carbon coatings around diamond clearly result from the post-shock annealing of diamond. For these reasons, we interpret the disordered carbon in NWA 4742 as a shock product, obtained by: (i) a partial and variable loss of structure of graphite, (ii) diamond back-transformation during post-shock annealing.

This could also be consistent for other ureilites, as strongly disordered carbon is the secondary carrier of noble gases, showing signatures close to diamond. The crystallographic relation between diamond and the disordered carbon demonstrated in this study explains these similarities.

5. CONCLUSION

We conclude from Raman microspectrometry (characterization at the micrometer scale) and HRTEM (characterization at the nanometre scale) observations of the various carbon phases in NWA 4742 and laboratory-shocked analogues that : (1) genetic relationships between diamond, distorted graphite and disordered carbon are common and can be explained by a late shock event; (2) at least part of (but probably not all) the diamond is directly formed from a graphite precursor, and not from strongly disordered material, for example organic matter; (3) organic-matter graphitization during internal heating (due to ^{26}Al decay for example) is a possible mechanism for graphite formation.

We demonstrate that, in NWA 4742, there is obviously a genetic link between phases at various scales and the associated nitrogen and noble gas signature should now be discussed in the light of these observations.

We suggest a three-stage generation history for NWA 4742 carbon material.

In a first event, diamond with noble gases would be produced from an undetermined precursor (possibly chondritic organic matter?) or environment (CVD-like hydrocarbon condensation). Shock or condensation origins are both plausible. If chondritic-like organics were the precursors of ureilites carbon, the graphitization of organic matter could be achieved during a post-accretion thermal event on the ureilite parent body at temperature lower than silicates melting temperatures. During the silicate melting episode, both diamond and graphite would be present together with CO/CO_2 fluids. Finally, in a later stage, a shock event large enough to produce diamond from graphite is proposed. This shock event would be responsible for the polycrystallinity of the diamond component and the genesis of the disordered carbon by shock-induced thermal back-transformation. This scenario would explain the noble gas content of the disordered carbon.

It is difficult at this point to link these episodes with the existing petrogenetic model of ureilites, and especially with the melting/smelting episodes. Nevertheless, the study of the various carbon phases identified in this work in other ureilites with various petrologic characteristics could help to unravel the genesis of these intriguing meteorites further.

ACKNOWLEDGMENTS

We are warmly thankful to Jun-Ichi Matsuda for providing the experimental shocked graphite samples. Nathaniel Findling from the Ecole Normale Superieure in Paris is acknowledged for both aquiring and processing the X-ray Diffraction data and Omar Boudouma (University Pierre and Marie Curie) is acknowledged for performing SEM imaging. Adrian Brearley and Christian Chopin are acknowledged for reading the manuscript and providing usefull corrections. Finally, we also want to thank C. Smith and D. Hezel for detailed and constructive reviews, as well as the associate editor C. Koeberl for encouraging comments.

REFERENCES

Amari S., Lewis R. S. and Anders E. (1994) Interstellar grains in meteorites: I. Isolation of SiC, graphite and diamond; size distributions of SiC and graphite. *Geochim. Cosmochim. Acta* **58**, 459–470.

Bachmann P. K., Leers D. and Lydtin H. (1991) Toward a general concept of diamond chemical vapor deposition. *Diamond Relat. Mater.* **1**, 1–12.

Banhart F. (1997) The transformation of graphitic onions to diamond under electron irradiation. *J. Appl. Phys.* **81**, 3440–3445.

Benedetti L. R., Nguyen J. H., Caldwell W. A., Liu H., Kruger M. and Jeanloz R. (1999) Dissociation of CH_4 at high pressures and temperatures: diamond formation in giant planet interiors? *Science* **286**, 100–102.

Bennett M. E. and McSween, Jr., H. Y. (1996) Revised model calculations for the thermal histories of ordinary chondrite parent bodies. *Meteorit. Planet. Sci.* **31**, 783–792.

Bény-Bassez C. and Rouzaud J. N. (1985) *Characterization of Carbonaceous Materials by Correlated Electron and Optical Microscopy and Raman Microspectrometry*. Scanning Electron Microscopy SEM Inc., Chicago, pp. 119–132.

Berkley J. L. and Jones J. H. (1982) Primary igneous carbon in ureilites: petrological implications. *J. Geophys. Res.* **87**, A353–A364.

Beyssac O., Goffé B., Chopin C. and Rouzaud J. N. (2002) Raman spectra of carbonaceous material in metasediments: A new geothermometer. *J. Metamorph. Geol.* **20**, 859–871.

Bhargava S., Bist H. D., Sahli S., Aslam M. and Tripathi H. B. (1995) Diamond polytypes in the chemical vapor deposited diamond films. *Appl. Phys. Lett.* **67**(12), 1706–1708.

Bischoff A., Goodrich C. A. and Grund T. (1999) Shock induced origin of diamonds in ureilites. *Lunar Planet. Sci.* XXX. Lunar Planet. Inst., Houston. #1100 (abstr.).

Bonal L., Quirico E., Bourot-Denise M. and Montagnac G. (2006) Determination of the petrologic type of CV3 chondrites by Raman spectroscopy of included organic matter. *Geochim. Cosmochim. Acta* **70**, 1849–1863.

Bonal L., Bourot-Denise M., Quirico E., Montagnac G. and Lewin E. (2007) Organic matter and metamorphic history of CO chondrites. *Geochim. Cosmochim. Acta* **71**, 1605–1623.

Bundy F. P. and Kasper J. S. (1967) Hexagonal diamond: a new form of carbon. *J. Chem. Phys.* **46**, 3437–3446.

Butenko Y. V., Kuznetsov V. L., Chuvilin A. L., Kolomiichuk V. N., Stankus S. V., Khairulin R. A. and Segall B. (2000) Kinetics of the graphitization of dispersed diamonds at "low" temperatures. *J. Appl. Phys.* **88**, 4380–4388.

Croat T. K., Stadermann F. J., Zinner E. and Bernatowicz T. J. (2004) Coordinated isotopic and TEM studies of presolar graphites from Murchison. *Lunar Planet Sci.* XVIII. Lunar Planet. Inst., Houston. #1353 (abstr.).

Daulton T. L., Eisenhour D. D., Bernatowicz T. J., Lewis R. S. and Buseck P. R. (1996) Genesis of presolar diamonds: comparative high resolution transmission electron microscopy study of meteoritic and terrestrial nano-diamonds. *Geochim. Cosmochim. Acta* **60**, 4853–4872.

De Barros M. I. and Vandenbulcke L. (2000) Plasma-assisted chemical vapor deposition process for depositing smooth diamond coatings on titanium alloys at moderate temperature. *Diamond Relat. Mater.* **9**, 1862–1866.

DeCarli P. S. (1998) Direct synthesis of diamond in the laboratory and in impact craters. *Meteorit. Planet. Sci.* **33**, A39.

DeCarli P. S. and Jamieson J. C. (1961) Formation of diamond by explosive shock. *Science* **33**, 1821–1822.

DeCarli P. S., Jones A. P., and Price G. D. (2002) Laboratory impact experiments and calculations versus natural impact events. In *Catastrophic events and mass extinctions: impacts and beyond*, (eds. C. Koeberl and K. G. MacLeod). GSA Special Paper 356. Geological Society of America, Boulder, Colorado. p. 746.

Downes H., Mittlefehldt D. W., Kita N. T. and Valley J. W. (2008) Evidence from polymict ureilite meteorites for a disrupted and re-accreted single ureilite parent asteroid gardened by several distinct impactors. *Geochim. Cosmochim. Acta* **72**, 4825–4844.

El Goresy A., Gillet P., Chen M., Künstler F., Graup G. and Stäle V. (2001) In situ discovery of shock-induced graphite-diamond phase transition in gneisses from the Ries Crater, Germany. *Am. Mineral.* **86**, 611–621.

El Goresy A., Dubrovinsky L. S., Gillet P., Mostefaoui S., Graup G., Drakopoulos M., Simionovici A. S., Swamy V. and Masaitis L. V. (2003) A new natural, super-hard, transparent polymorph of carbon from the Popigai impact crater, Russia. *C. R. Geosci.* **335**, 889–898.

Erskine D. J. and Nellis W. J. (1992) Shock-induced martensitic transformation of highly oriented graphite to diamond. *J. Appl. Phys.* **71**, 4882–4886.

Ferrari A. C. and Robertson J. (2000) Interpretation of Raman spectra of disordered and amorphous carbon. *Phys. Rev. B* **61**, 14095–14107.

Ferrari A. C. and Robertson J. (2001) Origin of the 1150-cm^{-1} Raman mode in nanocrystalline diamond. *Phys. Rev. B* **63**, R1–R4.

Franchi I. A., Sexton A. S., Wright I. P. and Pillinger C. T. (1997) Resolved sub-groups within the ureilite population. *Meteorit. Planet. Sci. Suppl.* **32**, 44.

Frenklach M., Kematick R., Huang D., Howard W., Spear K. E., Phelps A. W. and Koba R. (1989) Homogeneous nucleation of diamond powder in the gas phase. *J. Appl. Phys.* **66**, 395–399.

Frenklach M., Howard W., Huang D., Yuan J., Spear K. E. and Koba R. (1991) Induced nucleation of diamond powder. *Appl. Phys. Lett.* **59**, 546–548.

Frondel C. and Marvin U. B. (1967) Lonsdaleite, a hexagonal polymorph of diamond. *Nature* **214**, 587–589.

Fukunaga K., Matsuda J. I., Nagao K., Miyamoto M. and Ito K. (1987) Noble-gas enrichment in vapour-growth diamonds and the origin of diamonds in ureilites. *Nature* **328**, 141–143.

Göbel R., Ott U. and Begemann F. (1978) On trapped noble gases in ureilites. *J. Geophys. Res.* **83**, 855–867.

Gogotsi Y., Welz S., Ersoy D. A. and McNallan M. J. (2001) Conversion of silicon carbide to crystalline diamond-structured carbon at ambient pressure. *Nature* **411**, 281–287.

Goodrich C. A. (1992) Ureilites: a critical review. *Meteoritics* **27**, 327–352.

Goodrich C. A. (2008) Composition of ureilite precursor material. *Lunar and planetary science* XXXVIII, 1194 (abst.).

Goodrich C. A., Edward R. D. S. and Fiorettic A. M. (2004) Ureilitic breccias: clues to the petrologic structure and impact disruption of the ureilite parent asteroid. *Chemie der Erde* **64**, 283–327.

Goodrich C. A., Van Orman A. J. and Wilson L. (2007) Fractional melting and smelting on the ureilite parent body. *Geochim. Cosmochim. Acta* **71**, 2876–2895.

Goto T. and Syono Y. (1984) Technical aspect of shock compression experiments using the gun method. In *Material Science of the earth's Interior* (ed. I. Sunagawa), pp. 605–619. TERRAPUB.

Grady M. M., Wright I. P., Swart P. K. and Pillinger C. T. (1985) The carbon and nitrogen isotopic composition of ureilites: implications for their genesis. *Geochim. Cosmochim. Acta* **49**, 903–915.

Grady M. M. and Pillinger C. T. (1986) The ALHA82130 ureilites: its light element stable isotope composition and relationship to other ureilites. *Meteoritics* 21, 375–376 (abstr.).

Grady M. M. and Pillinger C. T. (1987) The ALHA82130 ureilites: its light element stable isotope composition and relationship to other ureilites. *Meteoritics* **21**, 375–376 (abstr.).

Grady M. M. and Pillinger C. T. (1988) ^{15}N-enriched nitrogen in polymict ureilites and its bearing on their formation. *Nature* **331**, 321–323.

Greshake A., Kenkmann T. and Schmitt R. T. (1999) *In situ* Raman spectroscopy of diamond in the ureilite Hammadahal Hamra 126. 63th *Annual Meteorit. Soc. Meeting*. #5049 (abstr.).

Grund T. and Bischoff A. (1999) Cathodoluminescence properties of diamonds in ureilites: further evidence for a shock induced origin. *62nd Annual Meteorit. Soc. Meeting*. #5074.

He H., Sekine T. and Kobayashi T. (2002) Direct transformation of cubic diamond to hexagonal diamond. *Appl. Phys. Lett.* **81**, 610–612.

Heymann D., Lipschutz M., Nielsen B. and Anders E. (1966) Canyon Diablo meteorite: metallographic and mass spectrometric study of 56 fragments. *J. Geophys. Res.* **71**, 619–641.

Hezel D. C., Dubrovinsky L., Nasdala L., Cauzid J., Simionovici A., Gellissen M. and Schönbeck T. (2008) In situ micro-Raman and X-ray diffraction study of diamonds and petrology of the new ureilite UAE 001 from the United Arab Emirates. *Meteorit. Planet. Sci.* **43**, 1127–1136.

Huo J., Songa H., Chen X., Zhao S. and Xu C. (2007) Structural transformation of carbon-encapsulated iron nanoparticles during heat treatment at 1000 °C. *Mater. Chem. Phys.* **101**, 221–227.

Huss R. G., Lewis R. S. and Hemkin S. (1996) The "normal planetary" noble gas component in primitive chondrites: compositions, carrier, and metamorphic history. *Geochim. Cosmochim. Acta* **60**, 3311–3340.

Jambon A., Barrat J. A., Boudouma O., Fonteilles M., Badia D., Göpel C. and Bohn M. (2005) Mineralogy and petrology of the angrite North West Africa 1296. *Meteorit. Planet. Sci.* **40**, 361–375.

Jehlicka J. and Rouzaud J. N. (1990) Organic geochemistry of Precambrian shales and schists (Bohemian Massif, Central Europe). *Org. Geochem.* **16**, 865–872.

Kagi H., Takahashi K., Shimizu H., Kitajima F. and Masuda A. (1991) In situ micro Raman studies on graphitic carbon in some Antartic ureilites. *Proc. NIPR Symp. Antart. Meteorit.* **4**, 371–383.

Karczemska A., Szurgot M., Kozanecki M., Szynkowska M. I., Ralchenko V., Danilenko V. V., Louda P. and Mitura S. (2008) Extraterrestrial, terrestrial and laboratory diamonds – Differences and similarities. *Diamonds Relat. Mater.* **17**, 1179–1185.

Langenhorst F., Shafranovsky G. I., Masaitis V. L. and Koivisto M. (1999) Discovery of impact diamonds in a Fennoscandian crater and evidence for their genesis by solid-state transformation. *Geology* **27**, 747–750.

Lapke C., Schmitt T.R., Kenkmann T. and Stöffler D. (2000) Raman microspectroscopy of impact diamonds from the Ries crater, Germany. 63th *Annual Meteorit. Soc. Meeting*. #5031 (abstr.).

Le Guillou C., Brunet F., Irifune T., Ohfuji H. and Rouzaud J. N. (2007) Nanodiamond nucleation below 2273 K at 15 GPa from carbons with different structural organizations. *Carbon* **45**, 636–648.

Le Guillou C., Rouzaud J. N., Findling N. and Düber S. (2009) Experimental graphitization and oxidation kinetic of nanodiamond: implication for nebular thermal processing. *40th Lunar and Planetary Science Conference*. #2070 (abstr.).

Lian W., Song H., Chen X., Li L., Huo J., Zhao M. and Wang G. (2008) The transformation of acetylene black into onion-like hollow carbon nanoparticles at 1000 °C using an iron catalyst. *Carbon* **46**, 525–530.

Lipschultz M. E. (1964) Origin of diamonds in ureilites. *Science* **143**, 1431–1434.

Mao L. W., Mao H., Eng J. P., Trainor T., Newville M., Kao C., Heinz D. L., Shu J., Meng Y. and Hemley R. J. (2003) Bonding changes in compressed superhard graphite. *Science* **302**, 425–427.

Matsuda J. I., Fukunaga K. and Ito K. (1991) Noble gas studies in vapor-growth diamonds: comparison with shock produced diamonds and the origin of diamonds in ureilites. *Geochim. Cosmochim. Acta* **55**, 2011–2023.

Matsuda J. I., Kusumi A., Yajima H. and Syono Y. (1995) Noble gas studies in diamonds synthesized by shock loading in the laboratory and their implications on the origin of diamonds in ureilites. *Geochim. Cosmochim. Acta* **59**, 4939–4949.

Mermoux M., Tajani A. T., Marcus B., Bustarret E., Gheeraert E., Nesladek M. and Koizumi S. (2004) Characterization of <1 1 1> diamond thin films by micro-Raman spectroscopy. *Diamond Relat. Mater.* **13**, 886–890.

Michaelson S., Ternyak O., Hoffman A. and Lifshitz Y. (2006) Hydrogen incorporation processes in nanodiamond films studied by isotopic induced modifications of Raman spectra. *Appl. Phys. Lett.* **89**, 131918.

Mittlefehldt D. W., Mc Coy T. J., Goodrich C. A. and Kracher A. (1998) Non-chondritic meteorites from asteroidal bodies. In *Planetary Materials* (ed. J. J. Papike). Mineralogical Society of America.

Miyamoto M., Matsuda J. and Ito K. (1988) Raman spectroscopy of diamond in ureilite and implication for the origin of diamond. *Geophys. Res. Lett.* **15**, 1445–1448.

Miyamoto M., Takase T. and Mitsuda Y. (1993) Raman spectra of various diamonds. *Mineral. J.* **16**, 246–257.

Morris D. G. (1980) An investigation of the shock-induced transformation of graphite to diamond. *J. Appl. Phys.* **51**, 2059–2065.

Murty S. V. S., Rai V. K. and Ott U. (1999) Nitrogen and noble gases in the diamond free ureilite Allan Hills 78019. *Meteorit. Planet. Sci.* 34, #85 (abstr.).

Nakamuta Y. and Aoki Y. (2000) Mineralogical evidence for the origin of diamond in ureilites. *Meteorit. Planet. Sci.* **35**, 487–493.

Oh J. H., Deubergue A., Rouzaud J. N., Oberlin A. and Kwak Y. H. (1991) Structural study of graphitization in the Mungyong Coalfield, South Korea. *Bull. Soc. Géol. Fr.* **162**(2), 399–407.

Onodera A. and Irie Y. (1991) Graphitization of amorphous carbon at high pressure to 15 GPa. *J. Appl. Phys.* **69**, 2611–2617.

Ott U., Löhr H. P. and Begemann F. (1984) Ureilites: the case of missing diamonds and a new neon component. *Meteoritics* **19**, 287–288 (abstr.).

Ott U., Löhr H. P. and Begemann F. (1985) Trapped noble gases in 5 more ureilites and the possible role of Q. *Lunar and Planet. Sci.* XVI. Lunar Planet. Inst., Houston. 639–640 (abstr.).

Ott U., Löhr H. P. and Begemann F. (1986) Noble gases in ALH82130: comparison with ALH 78019 and diamond-bearing ureilites. *Meteoritics* **21**, 477–478.

Ownby P. D., Yang X. and Liu P. J. (1992) Calculated X-ray diffraction data for diamond polytypes. *J. Am. Soc.* **75**, 1876–1883.

Quirico E., Raynal P.-Y. and Bourot-Denise M. (2003) Metamorphic grade of organic matter in six unequilibrated ordinary chondrites. *Meteorit. Planet. Sci.* **38**, 795.

Raï V. K., Murty V. S. and Ott U. (2003a) Nitrogen components in ureilites. *Geochim. Cosmochim. Acta* **67**, 2213–2237.

Raï V. K., Murty V. S. and Ott U. (2003b) Noble gases in ureilites: cosmogenic, radiogenic, and trapped components. *Geochim. Cosmochim. Acta* **67**, 4435–4456.

Rodríguez-Carvajal, J. 2001. An Introduction to the Program Fullprof 2000, Gif sur Yvette.

Russell S. S., Arden J. W., Franchi I. A. and Pillinger C. T. (1993) A carbon and nitrogen isotope study of carbonaceous vein material in ureilites. *Lunar Planet. Sci.* XXIV. Lunar Planet. Inst., Houston. 1221–1222 (abstr.).

Sadezky A., Muckenhuber H., Grothe H., Niessner R. and Pöschl U. (2005) Raman microspectroscopy of soot and related carbonaceous materials: spectral analysis and structural information. *Carbon* **43**, 1731–1732.

Setaka N. (1987) Vapor deposition of diamond. In *Proc Tenth Int. Conf. Chem. Vapor Deposition* (eds. G. W. Cullen and J. Blocher Jr.). Electrochemical Society, pp. 1156–1163.

Setaka N. (1989) Diamond synthesis from vapor phase and its growth process. *J. Mater. Res.* **4**, 664–670.

Shröder R. E., Nemanich R. J. and Glass J. T. (1990) Analysis of the composite structures in diamond thin films by Raman spectroscopy. *Phys. Rev. B* **41**, 3738–3745.

Smith D. K. (1989) Modern powder diffraction. In *Review in Mineralogy*, vol. 20 (eds. D. L. Bish and J. E. Post). Mineralogical Society of America, pp. 202–216.

Smith C. L., Franchi I. A., Wright I. P., Grady M. M. and Pillinger C. T. (2001) Ureilite graphite: shocking implications. 64th *Ann. Met. Soc. Meeting*. #5366 (abstr.).

Stöffler D., Keil K. and Edward S. R. D. (1991) Shock metamorphism of ordinary chondrites. *Geochim. Cosmochim. Acta* **55**(12), 3845–3867.

Takeda H., Ishii T., Otsuki M., Nakamuta T. and Nakamura T. (2001) Mineralogy of a newly weakly shocked ureilite Dar Al Gany 868 with diamonds. 64th *Ann. Met. Soc. Meeting*. #203 (abstr.).

Tan P., Deng Y. M. and Zhao Q. (1998) Temperature-dependent Raman spectra and anomalous Raman phenomenon of highly oriented pyrolytic graphite. *Phys. Rev. B* **58**, 5435–5439.

Tan P., Hu C. Y., Dong J. and Shen W. C. (2001) Polarization properties, high-order Raman spectra, and frequency asymmetry between Stokes and anti-Stokes scattering of Raman modes in a graphite whisker. *Phys. Rev. B* **62**, 214301-1–214301-12.

Tuinstra F. and Köenig J. L. (1970) Raman spectra of graphite. *J. Chem. Phys.* **53**, 1123–1130.

Valter A. A., Oleynik H. S., Fisenko A. V. and Semenova L. F. (2000) Electron microscopy evidences of Novo Urei diamond nature. *Lunar Planet. Sci.* XXXI. Lunar Planet. Inst., Houston. #1075 (abstr.).

Vandenbulcke L., Gries T. and Rouzaud J. N. (2009) Nanodiamonds in dusty low-pressure plasmas. *Appl. Phys. Lett.* **94**(4), 044106.

Vdovykin G. P. (1970) Ureilites. *Space Sci. Rev.* **10**, 483–510.

Wopenka B. and Pasteris J. D. (1993) Structural characterization of kerogens to granulite-facies graphite: applicability of Raman microprobe spectroscopy. *Am. Mineral.* **78**, 533–557.

Yagi T. and Utsumi W. (1992) High pressure in situ X-ray-diffraction study of the phase transformation from graphite to hexagonal diamond at room temperature. *Phys. Rev. B* **46**, 6031–6039.

Yamada K. and Tanabe Y. (2002) Shock-induced phase transition of oriented pyrolytic graphite to diamond at pressures up to 15 GPa. *Carbon* **40**, 261–269.

Yamada K., Burkhard G., Tanabe Y. and Sawaoka A. B. (1999) Nanostructure and formation mechanism of proto diamond shock-synthesized from graphite. *Carbon* **37**, 275–280.

Yoshikawa M., Mori Y., Maegawa M., Katagiri G., Ishida H. and Ishitani A. (1995) Raman scattering from diamond particles. *Appl. Phys. Lett.* **62**, 3114–3116.

Zhao X. Z., Cherian K. A., Roy R. and White W. B. (1998) Downshifts of Raman peak in diamond powders. *J. Mater. Res.* **13**, 1974–1977.

Associate editor: Christian Koeber